nature nanotechnology

LETTERS

PUBLISHED ONLINE: 4 MAY 2014 | DOI: 10.1038/NNANO.2014.82

Nanoscale temperature measurements using non-equilibrium Brownian dynamics of a levitated nanosphere

J. Millen[1]*, T. Deesuwan[2,3], P. Barker[1] and J. Anders[1,3]*

Einstein realized that the fluctuations of a Brownian particle can be used to ascertain the properties of its environment[1]. A large number of experiments have since exploited the Brownian motion of colloidal particles for studies of dissipative processes[2,3], providing insight into soft matter physics[4–6] and leading to applications from energy harvesting to medical imaging[7,8]. Here, we use heated optically levitated nanospheres to investigate the non-equilibrium properties of the gas surrounding them. Analysing the sphere's Brownian motion allows us to determine the temperature of the centre-of-mass motion of the sphere, its surface temperature and the heated gas temperature in two spatial dimensions. We observe asymmetric heating of the sphere and gas, with temperatures reaching the melting point of the material. This method offers opportunities for accurate temperature measurements with spatial resolution on the nanoscale, and provides a means for testing non-equilibrium thermodynamics.

Brownian motion is an essential tool for the investigation of micro- and nanoscale properties and processes in the physical and life sciences. Experiments are now at the nanoscale, where single particles can be strongly trapped by optical tweezers, electrostatic and magnetic traps[9,10]. The precise control offered by these techniques has made possible the experimental observation of physical phenomena at previously inaccessible scales. These include measurement of the non-Gaussian nature of fluids[2] and the verification of Landauer's principle[3], which links thermodynamics with information theory. Trapping methods have also allowed the observation of biomolecular forces[4,5], the accurate determination of nanoscale particle properties (such as charge and size[11]) and the characterization of potential landscapes when modified by colloidal interactions[6], for example. These experiments have focused on the motion of the particle and its interaction with the bath. However, the substantial impact of the surface temperature of a trapped particle on its dynamics has only recently been studied[12,13]. The dynamics of colloidal particles undergoing hot Brownian motion in a liquid has been characterized by an effective diffusion constant[12], and spatial asymmetry in the diffusion was shown to enable active Brownian motion[14,15]. However, the observation of hot Brownian dynamics in a gas, where very large temperature differences can be present, has not been explored. Here, we report on the measurement of the modified Brownian motion of a strongly heated trapped nanosphere in the underdamped (Knudsen) regime, which produces a non-equilibrium gas around it. A schematic of the experiment is shown in Fig. 1a, and a photograph of the trap in Fig. 1b.

When the temperature of the surface of a sphere is different from its surrounding gas, for example when it is heated by the absorption of light, heat is transferred to the colliding gas particles. Impinging gas particles at temperature T^{imp} do not in general equilibrate to the same temperature as the sphere surface at temperature T_{sur} (partial accommodation[16]). They emerge with a different energy and can be assumed to be thermally distributed for highly inelastic collisions[17], with an emerging temperature $T^{\mathrm{em}} \neq T^{\mathrm{imp}}$ (Fig. 1c). This change in temperature implies that the gas is not in thermal equilibrium, as assumed in the analysis of most optical tweezer experiments. In contrast, we derive a model of modified Brownian motion based on two non-interacting baths, the impinging gas at temperature T^{imp} and the emerging gas at T^{em}, which interact with the sphere's centre-of-mass motion (see Supplementary Section A 'Impinging and emerging gas model'). This situation only occurs in the Knudsen regime, where the mean free path of the gas is much larger than the sphere radius and hence the gases do not equilibrate in the vicinity of the sphere. The sphere's centre-of-mass motion adopts a non-equilibrium steady state that mediates heat transfer between the two baths. Importantly, even though the gas is not in equilibrium, the power spectrum of the sphere's fluctuating position is of the thermal form $P(\omega) = (2k_{\mathrm{B}}T_{\mathrm{CM}}/M) \cdot \Gamma_{\mathrm{CM}}/((\omega_0^2 - \omega^2)^2 + \omega^2\Gamma_{\mathrm{CM}}^2)$, where k_{B} is the Boltzmann constant, M is the mass of the sphere and ω_0 is its trap frequency. The power spectrum is parameterized by an effective centre-of-mass temperature, $T_{\mathrm{CM}} = (T^{\mathrm{imp}}\Gamma^{\mathrm{imp}} + T^{\mathrm{em}}\Gamma^{\mathrm{em}})/(\Gamma^{\mathrm{em}} + \Gamma^{\mathrm{imp}})$ and an effective damping rate, $\Gamma_{\mathrm{CM}} = \Gamma^{\mathrm{em}} + \Gamma^{\mathrm{imp}}$.

To study the Brownian fluctuations in thermal non-equilibrium we used silica spheres with diameters of 105.1 nm and 2.56 μm in a dual-beam optical trap with a wavelength of 1,064 nm. Silica can be heated as a result of the absorption of trap light by impurities in the material. At any given pressure, the temperature of the spheres can be controlled by the laser light intensity with an approximately linear dependence[18], $T_{\mathrm{sur}} \propto I$. In the steady state, T_{sur} is determined by the balance between heating due to laser absorption and cooling due to collisions with the gas and the emission of blackbody radiation. The exact rate of heating depends on the prevalence of impurities within the material and thus varies from sphere to sphere. Even though absorption is low, high temperatures (~2,000 K) can be reached because of poor heat transfer to the surrounding gas at low pressures.

The optical trap is well approximated by a three-dimensional harmonic potential with frequencies in the direction along the laser focus (ω_z) and those orthogonal to it (ω_x and ω_y). Frequencies range from ~1 kHz to 15 kHz and depend on laser intensity, the axis of motion and particle size. The trap was placed inside a vacuum chamber and the motion of the particle was monitored (see Methods) in two spatial directions—axial (z) and radial (x)—using a quadrant photodetector (QPD, Fig. 1a). The particles were stable in the trap for many hours.

[1]Department of Physics and Astronomy, University College London, Gower Street, London WC1E 6BT, UK, [2]Department of Physics, Imperial College London, Prince Consort Road, London SW7 2AZ, UK, [3]Department of Physics and Astronomy, University of Exeter, Stocker Road, Exeter EX4 4QL, UK.
*e-mail: j.millen@ucl.ac.uk; janet@qipc.org

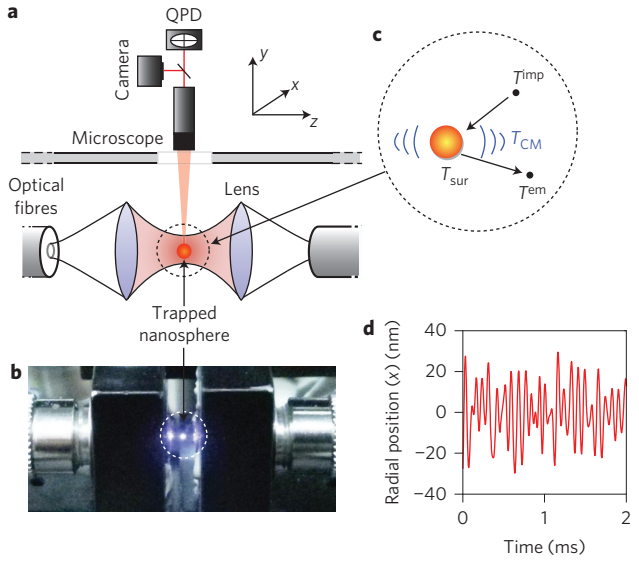

Figure 1 | Experimental schematic and photograph of levitation experiment. a, Silica spheres are levitated in a dual-beam optical tweezer inside a vacuum chamber. Light of wavelength 1,064 nm is coupled into lenses from single-mode optical fibres, creating an optical trap. The motion of the levitated sphere is monitored with a camera and a QPD. **b**, Photograph of the trapping region with the trapped sphere visibly scattering trap light. **c**, Schematic showing the temperatures involved in a collision with a heated sphere: the sphere's centre-of-mass temperature (T_{CM}) and surface temperature (T_{sur}), and the temperatures of the impinging gas particles (T^{imp}) and emerging gas particles (T^{em}) with $T^{imp} \leq T_{CM} \leq T^{em} \leq T_{sur}$. **d**, Typical Brownian motion position trace for a 105.1 nm sphere at 1 mbar.

We varied the laser intensity from 0.3 to 15 MW cm^{-2} and lowered the pressure of the gas in the chamber from atmospheric to ~1 mbar. The radial position of a 105.1-nm-diameter sphere as a function of time at 1 mbar is depicted in Fig. 1d, showing the harmonic motion with Brownian fluctuations. From the axial and radial position data we calculated and fit the autocorrelation function (Fig. 2a) and power spectra (Fig. 2b). Fitting the experimental power spectra to $P(\omega)$ allows the determination of the effective damping coefficient $\Gamma_{CM}/(2\pi)$ and the prefactor $A = (2k_B T_{CM})/M$ for each spatial direction once a voltage-to-position calibration factor has been determined for the QPD (see Methods). With this method the ratio of the effective temperature (T_{CM}) over mass (M) can be determined for any laser intensity and pressure. As expected, the trap frequency increases with increasing laser intensity (Fig. 2c). In addition, the sphere's centre-of-mass motion experiences a substantial increase in temperature (Fig. 2c) when compared to power spectra at increased frequency but remaining at the initial temperature.

With the measured centre-of-mass temperature T_{CM}, the temperature of the emerging gas particles, T^{em}, can be deduced using the fact that the gas particles impinge at room temperature, $T^{imp} = 294$ K. Also needed to extract T^{em} is the damping rate due to the emerging gas, which we derive in the Supplementary Section B. This is given by $\Gamma^{em} = \frac{\pi}{8}\sqrt{T^{em}/T^{im}}\,\Gamma^{imp}$, where $\Gamma^{imp} = (4\pi/3)\,(mNR^2\bar{v}_{T^{imp}}/M)$, m is the molecular mass, $\bar{v}_{T^{imp}} = \sqrt{(8k_B T^{imp}/\pi m)}$ is the mean thermal velocity, N is the gas particle density and R is the sphere radius[17]. The temperature of the emerging gas particles can now be found by solving $T_{CM} = ((T^{imp})^{3/2} + \frac{\pi}{8}(T^{em})^{3/2})/((T^{imp})^{1/2} + \frac{\pi}{8}(T^{em})^{1/2})$ for T^{em}.

Figure 3a,b shows the inferred temperature of the emerging gas surrounding 2.56-μm- and 105.1-nm-diameter spheres as a function of laser intensity. The typical accuracy of the temperature measurement is 10%. For the 2.56 μm sphere (Fig. 3a), strong gas heating is always observed at 1 mbar, while no measurable heating occurs at 5 mbar. In the latter case, the more frequent collisions of the sphere with gas particles take heat away from the sphere surface more efficiently. This prevents heating of the sphere surface and the gas emerging from it. Because the larger spheres act as a lens for the trapping light, a non-uniform intensity profile is expected within it. This is illustrated by our simulations, shown in Fig. 3c, using generalized Lorentz–Mie theory and the Optical Tweezers Toolbox[19]. For particles of this size one therefore expects an asymmetric surface temperature, which would lead to a higher on-axis temperature of the emerging gas particles. Indeed, we measure a considerably larger temperature in the axial direction than in the radial direction (Fig. 3a), giving unambiguous evidence that at 1 mbar the large sphere is moving through two baths, the impinging gas at room temperature and the emerging gas with spatially varying temperature.

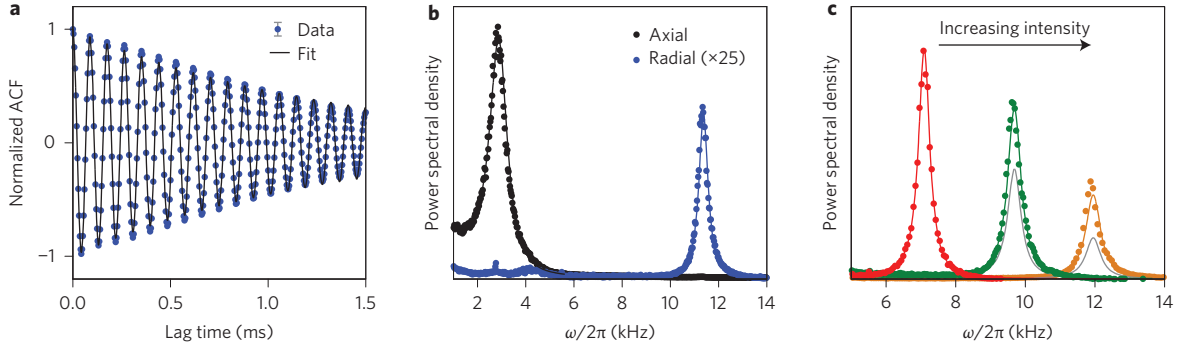

Figure 2 | Two-dimensional Brownian motion and its variation with trap laser intensity. All displayed data are for 105.1 nm spheres at 1 mbar. **a**, Autocorrelation function (ACF) of experimentally measured radial position (blue points with grey error bars) and fit with theory (black solid line) (Supplementary equation (4)). **b**, Measured axial (black points) and radial (blue points) position power spectra with fits to $P(\omega)$ (solid lines) over trap frequency $\omega/2\pi$. Because of the low damping at mbar pressures, the axial (z) and radial (x) peak frequencies, $\tilde{\omega}_{x,z} = \sqrt{\omega_{x,z}^2 - \Gamma_{CM}^2/2}$, approximate the trap frequencies $\omega_{x,z}$. **c**, Measured radial power spectra (points) with fits (solid lines) for three values of trapping laser intensity. From left to right the intensity of the trapping laser beams is increased by a factor of 2.1 and the peak frequency $\tilde{\omega}_x/2\pi$ increases with intensity, as expected. If there were no temperature increase from the initial intensity (red), the peak height would behave as indicated by the grey solid lines. However, it can be seen that the height of the peak, $A/\Gamma_{CM}\omega_x^2 = 2k_B T_{CM}/M\Gamma_{CM}\omega_x^2$, increases with intensity in comparison to the grey lines, indicating the increase of the centre-of-mass temperature, T_{CM}, of the sphere.

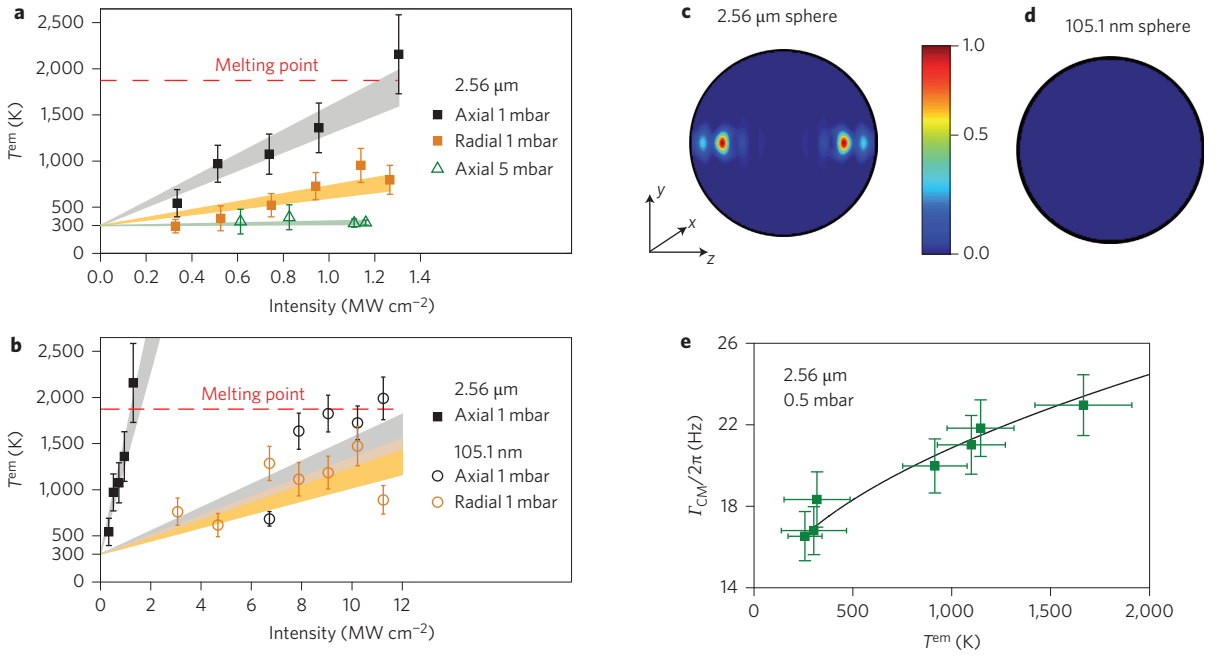

Figure 3 | Analysis of heating as a function of pressure, spatial direction and sphere size. a, Temperature of emerging gas particles (T^{em}) with trapping laser intensity for the large spheres in the axial (black squares) and radial (orange squares) directions at 1 mbar, and in the axial direction at 5 mbar (green triangles). Asymmetric heating is observed at 1 mbar, but no heating occurs at 5 mbar. The shaded areas show linear fits with one standard deviation of uncertainty indicating that a linear relationship $T^{em} \propto T_{sur} \propto I$ holds, as expected[18]. **b**, Temperature of emerging gas particles versus trapping laser intensity for 105.1-nm-diameter (open circles) and 2.56-μm-diameter (filled squares) spheres at 1 mbar in axial (black) and radial (orange) directions. Heating of the gas is clearly observed for both large and small spheres. Shaded areas indicate linear fits with one standard deviation of uncertainty as a guide to the eye. The red dashed lines in **a**,**b** indicate the melting temperature of silica (1,873 K; see ref. 20). At intensities beyond the shown data points the spheres leave the trap. **c**, Field intensity inside the 2.56 μm spheres for two incident counterpropagating Gaussian beams, clearly showing lensing of the light. **d**, Field intensity inside the 105.1 nm spheres for two incident counterpropagating Gaussian beams, showing homogeneous intensity throughout the spheres. **e**, Measured variation (green squares) of the damping coefficient Γ_{CM} for a 2.56-μm-diameter sphere at 0.5 mbar versus temperature of the emerging gas particles, T^{em}. Also shown is the theoretical Γ_{CM} (black solid line) with no free parameters, using the experimentally given parameters $T^{imp} = 294$ K and $\Gamma^{imp} = 76.3$ Hz for 2.56 μm spheres.

The gas surrounding the smaller spheres generally experiences a much slower heating than that around the larger spheres (Fig. 3b). This can be understood by realizing that while cooling mechanisms such as collisions and blackbody radiation scale with surface area, heating due to absorption from the laser beam scales with volume. Heating depends on the number of impurities in the material, and the smaller spheres show a much more varied heating pattern than the larger spheres. The data presented in Fig. 3b show one of the strongest examples of heating observed for the small spheres. In contrast to the larger spheres, no lensing effects should occur for the smaller 105.1 nm spheres, as shown by our simulation (Fig. 3d). This agrees well with the experimental data, which do not indicate significant spatial asymmetry (Fig. 3b).

Figure 3e shows the variation of the damping coefficient Γ_{CM} with emerging gas temperature T^{em}, together with the theoretical result for Γ_{CM}. The plot is obtained without any fitting parameters, showing the consistency of the theoretical prediction. In Fig. 3b, data points are shown for the large and small spheres up to a maximum intensity. Beyond these intensities the spheres are heated so strongly that they melt and leave the trap, thus rendering further data points impossible. The temperatures corresponding to the highest observable intensities for both sphere sizes are consistent with the literature value of the melting temperature of silica (given as 1,873 K (ref. 20)), which is indicated by the red dashed lines in Fig. 3a,b. This independently verifies the measured emerging gas temperatures.

The relationship between the gas temperatures and the surface temperature of the sphere is given by a material constant, the accommodation coefficient $\alpha = (T^{em} - T^{imp})/(T_{sur} - T^{imp})$. The accommodation coefficient for silica is known[21], and is close to 0.777 for moderate surface temperatures around 300 K. This allows us to infer the surface temperature of the nanospheres, $T_{sur} = 294\,K + (T^{em} - 294\,K)/0.777$. At high temperatures the accommodation coefficient is not known, and the emerging gas temperature establishes a lower bound on the surface temperature. However, independent measurements of the surface temperature (based on the emitted blackbody radiation) are possible in this regime[22], which would allow the determination of the variation of the accommodation coefficient.

Finally, experiments with levitated particles, both old[23] and new[24,25], have faced difficulties reaching low pressures, and it has widely been believed that heating plays a part in this[23,25]. Our data suggest that heating is the dominant cause for the loss of larger particles from the trap at pressures higher than ~1 mbar. However, temperature-independent mechanisms also play an important role. As already indicated for Fig. 3a, at high enough intensities the 2.56 μm spheres melt and vanish from the trap. Such loss is also evidenced by a marked rise of the measured minimum pressure at which the spheres can still be trapped with increasing intensity, as seen in Fig. 4a. In addition, we observe that at fixed laser intensity the level of light scattered from the spheres decays strongly when the pressure is reduced (Fig. 4b), indicating that evaporation occurs. The 105.1 nm spheres may also melt at very high intensities, as indicated in Fig. 3b, but the loss of these spheres at lower intensities and low pressures is the result of a temperature-independent mechanism, as evidenced in Fig. 4a,b. For example, parametric

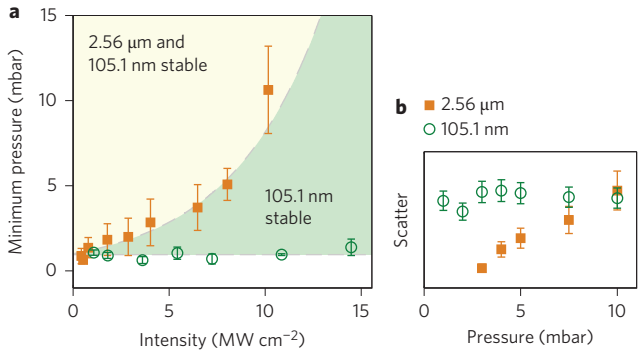

Figure 4 | Minimum attainable pressure. a, Minimum pressure for which 2.56 μm (orange squares) and 105.1 nm (green circles) spheres were stably trapped versus intensity. These data are averaged over different spheres of each size (>5) at each intensity. Owing to their strong heating, the 2.56 μm spheres evaporate at high intensities, leading to an intensity-dependent attainable pressure. In contrast, the smaller spheres are lost below an average pressure of 0.95 mbar, regardless of the laser intensity. **b**, Scatter plot versus pressure at fixed intensity 1.3 MW cm^{-2}, showing the total scattered light intensity from the 2.56 μm spheres (orange squares) and 105.1 nm spheres (green circles). At lower pressure, the scatter drops strongly for the 2.56 μm spheres, indicating that they have evaporated to a smaller size, while the 105.1 nm spheres show an approximately constant scatter.

heating, which results from any noise in the system (such as laser noise and vibrations), can render the trap unstable. Consistent with this interpretation, it was observed[24] that at low trap laser intensities the limiting pressure is independent of size for a range of sphere diameters from 50 nm to 2.56 μm. It is known that feedback cooling is a reliable method well suited to correct for parametric heating[26,27].

We have derived and tested a model for the Brownian motion of a particle in a non-equilibrium gas in the Knudsen regime. Using an optically levitated nanosphere we performed measurements of the temperature of the non-equilibrium gas surrounding the sphere at mbar pressures with a typical precision of 10%. The experiment allowed us to observe substantial heating of the gas particles emerging from the sphere surface, even for modest trapping laser intensities. Our method can also be used with other trapping techniques, such as electrostatic or magnetic levitation[9], where the particle is heated by other means. An anisotropic temperature distribution of the gas surrounding the larger spheres was found, giving testimony to the non-equilibrium nature of the sphere's centre-of-mass motion. We achieved a spatial resolution of ∼100 nm, which is greater than that of standard optical imaging techniques.

While the fluctuations of the sphere were used here to provide information about the bath, they are also a means with which to determine the properties of the trapped sphere, including its surface temperature and its accommodation coefficient. Our results show that a careful distinction between the operating temperature (for example, room temperature), the spatially varying surface temperature and the sphere's three centre-of-mass temperatures must be considered in any optical tweezer experiment. This is particularly relevant for recent experiments and proposals[26–29] to cool the centre-of-mass motion of optically levitated particles with the aim of reaching the quantum ground state. Using nanospheres as a local probe of bath properties in other non-equilibrium environments in the Knudsen regime is a promising tool for micro-rheology[30], microfluidics[31] and for the study of aerosols[25]. For instance, with nanospheres of smaller size (∼10 nm), this method could be used at nearly atmospheric pressures. The presented approach also opens up opportunities for exploring the intermediate regime between the limiting cases of the dilute gas and dense fluid. This transition can be measured with a methodology based on our technique and observations of timescales of equilibration in the gas, and the onset of memory effects[2] could be investigated. Finally, the presented approach provides a starting point for investigations of non-equilibrium thermodynamics extending into the underdamped regime, such as testing fluctuation theorems, studying stochastic thermodynamics[32] and entropy production[13], and exploring the link between thermodynamics and information theory[3].

Methods

Trap set-up and characterization. Silica spheres of diameter 105.1 nm (Corpuscular) and 2.56 μm (Bangs Labs) were trapped. The trap light was split into two beams of equal power by an acousto-optic modulator (AOM), introducing a frequency difference of 80 MHz and eliminating interference effects in the trap. These two beams were coupled into separate single-mode optical fibres, which entered a vacuum chamber, with the output focused by aspherical lenses of focal length 1.45 mm to create a trap with a beam waist of ∼1 μm. One of the fibre-lens systems was mounted on a translation stage, allowing alignment in three dimensions. The spheres were introduced to the trapping region using a nebulizer (Omron NEU22) at atmospheric pressure, as the damping force of the air was required to load the trap. The spheres were suspended in methanol with very low particle concentration, and the solution was sonicated in an ultrasonic bath for at least an hour before trapping to prevent clumping.

Monitoring. The trapped particle was monitored from outside the vacuum chamber by a CMOS camera (for diagnostics) and a QPD using a microscope with a zoom of ×45 (Fig. 1a). The detectors picked up scattered trapping light. When very low trap light intensities were required (for the 2.56 μm spheres), a weak beam of 532 nm was used to illuminate the sphere, with an intensity of ∼0.5 kW cm^{-2}, as the detector is more sensitive at this wavelength. The QPD allowed us to monitor the position fluctuations of the trapped sphere in the axial (z) and radial (x) directions. The orthogonal direction (y) offers the same trapping landscape as the radial direction when the system is well aligned. Because the QPD measures intensity fluctuations on its pixels as the particle moves, we were able to measure movement with nanometre resolution.

Data acquisition and analysis. The pressure in the trap was measured with 15% accuracy with a Pirani and Bourdon gauge. The trapping light intensity was varied with an AOM and also monitored by collecting light scattered by the sphere. An oscilloscope recorded the motion of each trapped sphere at a fixed pressure for 20 s, with a time resolution of 4 μs. The power spectral density $P(\omega)$ of the motional data was calculated and analysed using the equation given above, with an additional constant-valued fitting parameter to account for a non-zero background. To calibrate the QPD, data sets were taken at high enough pressures that no variation of T_{CM} with laser intensity was observed, indicating that the gas surrounding the sphere was in thermal equilibrium at room temperature (294 K). Each nanosphere behaved in a different way as a result of variations in manufacture. This means that, for a given intensity and pressure, different spheres of the same size will reach different temperatures. However, the trends are consistent across all realizations.

Theoretical model. The sphere interacts in each spatial direction, x, with two independent baths, the impinging gas and the emerging gas. Collisions between the gas particles and the sphere are inelastic since the sphere has a large accommodation coefficient. The gas particles stick on the surface and emerge independent in time and energy from the impinging gas particles. Both the impinging and emerging gas are assumed thermally distributed[17], with temperatures T^{imp} and T^{em}, respectively. The sphere experiences effective damping force against its motion with damping coefficient $\Gamma_{\mathrm{CM}} = \Gamma^{\mathrm{imp}} + \Gamma^{\mathrm{em}}_x$, with the known[17] impinging damping coefficient Γ^{imp}. For the emerging gas damping coefficient we considered the total drag force due to each leaving particle on the sphere moving with velocity V in three dimensions,

$$F^{\mathrm{em}}_{\mathrm{drag}} = \int_0^{\pi}\int_0^{2\pi} \frac{mN\sqrt{\pi}\cos\theta\, V}{4\sqrt{(m/2k_{\mathrm{B}}T^{\mathrm{em}})}}\cos\theta\,\mathrm{d}S,$$

from which we obtained $\Gamma^{\mathrm{em}} = F^{\mathrm{em}}_{\mathrm{drag}}/MV$. Details of the derivation are given in the Supplementary Information.

Received 5 August 2013; accepted 21 March 2014; published online 4 May 2014

References

1. Einstein, A. Über die von der molekularkinetischen Theorie der Wärme geforderte Bewegung von in ruhenden Flüssigkeiten suspendierten Teilchen. *Ann. Phys. (Berlin)* **322,** 549–560 (1905).

2. Franosch, T. *et al.* Resonances arising from hydrodynamic memory in Brownian motion. *Nature* **478,** 85–88 (2011).
3. Bérut, A. *et al.* Experimental verification of Landauer's principle linking information and thermodynamics. *Nature* **483,** 187–189 (2012).
4. Guydosh, N. R. & Block, S. M. Direct observation of the binding state of the kinesin head to the microtubule. *Nature* **461,** 125–128 (2009).
5. Ashkin, A., Dziedzic, J. M. & Yamane, T. Optical trapping and manipulation of single cells using infrared laser beams. *Nature* **330,** 769–771 (1987).
6. Tischer, C. *et al.* Three-dimensional thermal noise imaging. *Appl. Phys. Lett.* **79,** 3878–3880 (2001).
7. Hänggi, P. & Marchesoni, F. Artificial Brownian motors: controlling transport on the nanoscale. *Rev. Mod. Phys.* **81,** 387–442 (2009).
8. Le Bihan, D. *et al.* MR imaging of intravoxel incoherent motions: application to diffusion and perfusion in neurologic disorders. *Radiology* **161,** 401–407 (1986).
9. Hinkle, L. D. & Kendall, B. R. F. Brownian motion of a particle levitated in vacuum. *J. Vac. Sci. Technol. A* **10,** 243–247 (1992).
10. Li, T., Kheifets, S., Medellin, D. & Raizen, M. G. Measurement of the instantaneous velocity of a Brownian particle. *Science* **328,** 1673–1675 (2010).
11. Mojarad, N. & Krishnan, M. Measuring the size and charge of single nanoscale objects in solution using an electrostatic fluidic trap. *Nature Nanotech.* **7,** 448–452 (2012).
12. Rings, D., Schachoff, R., Selmke, M., Cichos, F. & Kroy, K. Hot Brownian motion. *Phys. Rev. Lett.* **105,** 090604 (2010).
13. Ciliberto, S., Imparato, A., Naert, A. & Tanase, M. Heat flux and entropy produced by thermal fluctuations. *Phys. Rev. Lett.* **110,** 180601 (2013).
14. Palacci, J., Cottin-Bizonne, C., Ybert, Ch. & Bocquet, L. Sedimentation and effective temperature of active colloidal suspensions. *Phys. Rev. Lett.* **105,** 088304 (2010).
15. Jiang, H-R., Yoshinaga, N. & Sano, M. Active motion of a Janus particle by self-thermophoresis in a defocused laser beam. *Phys. Rev. Lett.* **105,** 268302 (2010).
16. Goodman, F. O. Thermal accommodation coefficients. *J. Phys. Chem.* **84,** 1431–1445 (1980).
17. Epstein, P. S. On the resistance experienced by spheres in their motion through gases. *Phys. Rev.* **23,** 710–733 (1924).
18. Peterman, E. J. G., Gittes, F. & Schmidt, C. F. Laser-induced heating in optical traps. *Biophys. J.* **84,** 1308–1316 (2003).
19. Nieminen, T. A. *et al.* Optical tweezers computational toolbox. *J. Opt. A* **9,** S196–S203 (2007).
20. http://www.azonano.com/article.aspx?ArticleID=3398.
21. Ganta, D., Dale, E. B., Rezac, J. P. & Rosenberger, A. T. Optical method for measuring thermal accommodation coefficients using a whispering-gallery microresonator. *J. Chem. Phys.* **135,** 084313 (2011).
22. Landström, L. & Heszler, P. Analysis of blackbody-like radiation from laser-heated gas-phase tungsten nanoparticles. *J. Phys. Chem. B* **108,** 6216–6221 (2004).
23. Ashkin, A. & Dziedzic, J. M. Optical levitation in high vacuum. *Appl. Phys. Lett.* **28,** 333–335 (1976).
24. Monteiro, T. *et al.* Dynamics of levitated nanospheres: towards the strong coupling regime. *New J. Phys.* **15,** 015001 (2013).
25. Burnham, D. R., Reece, P. J. & McGloin, D. Parameter exploration of optically trapped liquid aerosols. *Phys. Rev. E* **82,** 051123 (2010).
26. Li, T., Kheifets, S. & Raizen, M. G. Millikelvin cooling of an optically trapped microsphere in vacuum. *Nature Phys.* **7,** 527–530 (2011).
27. Gieseler, J., Deutsch, B., Quidant, R. & Novotny, L. Subkelvin parametric feedback cooling of a laser-trapped nanoparticle. *Phys. Rev. Lett.* **109,** 103603 (2012).
28. Chang, D. E. *et al.* Cavity opto-mechanics using an optically levitated nanosphere. *Proc. Natl Acad. Sci. USA* **107,** 1005–1010 (2010).
29. Romero-Isart, O., Juan, M. L., Quidant, R. & Cirac, J. I. Toward quantum superposition of living organisms. *New J. Phys.* **12,** 033015 (2010).
30. Bennett, J. S. *et al.* Spatially-resolved rotational microrheology with an optically-trapped sphere. *Sci. Rep.* **3,** 01759 (2013).
31. Enger, J., Goksör, M., Ramser, K., Hagberg, P. & Hanstorp, D. Optical tweezers applied to a microfluidic system. *Lab Chip* **4,** 196–200 (2004).
32. Seifert, U. Stochastic thermodynamics: principles and perspectives. *Eur. Phys. J. B* **64,** 423–431 (2008).

Acknowledgements

The authors thank I. Ford for discussions and I. Llorente Garcia, D. Duffy and I. Ford for critical reading of the manuscript. J.M. and P.B. acknowledge funding from the Engineering and Physical Sciences Research Council (EPSRC) of the UK (EP/H050434/1). T.D. is supported by the Royal Thai Government and the EPSRC. J.A. is supported by the Royal Society. This work was supported by the European COST network MP1209.

Author contributions

J.M. and P.B. designed the experiments. J.M. performed the experiments, analysed the data and performed error analysis. T.D and J.A. developed the two-bath model. J.A. derived the damping rate. P.B. performed the field simulation. All authors contributed to data analysis and wrote the manuscript.

Additional information

Supplementary information is available in the online version of the paper. Reprints and permissions information is available online at www.nature.com/reprints. Correspondence and requests for materials should be addressed to J.M. and J.A.

Competing financial interests

The authors declare no competing financial interests.